Theoretical study of structural stabilities and magnetic properties of doped transition metals in MnTe vs ZnTe and CdTe: Reduced clustering trend and enhanced magnetic coupling

Jian-Ming Wu,[1] Xing-Yuan Chen,[1] Shi-Yuan Lin,[1] and Yu-Jun Zhao[1,2,a)]
[1]*Department of Physics, South China University of Technology, Guangzhou 510640, People's Republic of China*
[2]*State Key Laboratory of Luminescent Materials and Devices, South China University of Technology, Guangzhou 510640, People's Republic of China*

(Received 7 May 2013; accepted 11 August 2013; published online 27 August 2013)

Clustering and weak magnetic coupling of doped transition metals (TMs) have hampered the potential spintronic applications of many magnetic semiconductors. Here, the influence of the host crystal magnetic background on the magnetic coupling and clustering of TM impurities is studied theoretically, with a comparison of a series of TMs (V, Cr, Fe, Co, and Ni) in MnTe, ZnTe, and CdTe hosts. We found that the antiferromagnetic (AFM) background of MnTe degrades the clustering tendency of the studied TM impurities (except Ni). Meanwhile, the AFM background of MnTe significantly enhances the magnetic coupling of doped Fe, Co, and Ni pairs in general, either ferromagnetically (for Fe, Ni) or antiferromagnetically (for Co). The enhanced ferromagnetic coupling and weakened clustering of Fe impurities in MnTe imply that an AFM background of host semiconductors may aid the development of high T_C magnetic semiconductors with intrinsic magnetism. © *2013 AIP Publishing LLC*. [http://dx.doi.org/10.1063/1.4819329]

I. INTRODUCTION

In the past decade, dilute magnetic semiconductor materials have attracted enormous interest because of their great potential applications in spintronic devices,[1,2] which make use of both the charge and spin properties of electrons. In early dilute magnetic semiconductor (DMS) studies, transition metals (TMs) were often introduced to routine nonmagnetic semiconductors as a magnetic resource.[3–8] After the report of GaMnAs materials having a Curie temperature (T_C) of 110 K,[1] Dietl and Ohno predicted high T_C in some Mn-doped wide-gap II–VI and III–V compounds with certain extended carriers.[9,10] Stimulated by those works, a flurry of investigations were carried out to push the T_C of DMSs up to room temperature (RT).[4,11–19] Ferromagnetism in GaMnAs cannot, however, be enhanced indefinitely by increasing the concentration of Mn ions, as some Mn ions will occupy interstitial sites or form clustered phases. The possibility of TM doping in other common semiconductors like zinc blende (ZB) MnTe,[20–22] ZnO,[23–27] CdTe,[28,29] GaN,[30] and TiO_2 (Ref. 31) has also been very attractive. Subsequent studies on wide-gap DMSs have resulted in many reports of RT-DMSs. However, the origin and the high T_C of ferromagnetism in DMSs are arguably the most controversial research topics in materials science and condensed matter physics of recent times.[32–36] It is believed that most of the reported experimental results were not well validated and are difficult to reproduce. Recently, Samarth[33] and Chambers[34] ascribed the origin of the ferromagnetism of DMSs to impurity clustering, secondary phases, or some other uncontrollable intrinsic defects. Based on first-principles studies, Zunger *et al.*[35] put forward some contradictory theoretical views on both the origin of ferromagnetism and the high T_C of the most widely reported DMSs.

It is now accepted that two essential aspects should be addressed in further investigations of DMS. One is the achievement of a uniform distribution of TM dopants to avoid clustering or secondary-phase formation, assuring an intrinsic ferromagnetic (FM) nature of the resulting DMSs. The other is the enhancement of magnetic exchange interactions between TM impurities, assuring a high T_C of stable FM or ferrimagnetic (Ferri) states in the DMSs.

Meanwhile, it is well known that iso-valence substitutional doping in semiconductors, such as Mn in CdTe,[37–39] can achieve a high impurity concentration without forming secondary phases, although antiferromagnetic (AFM) coupling is often favored. In fact, ZB-structured MnTe can be prepared experimentally, and there are many reports on MnTe:TMs with confirmed or predicted ferrimagnetism and half metallic properties.[14,22,40,41] This creates a new approach for DMSs via the doping of TMs in semiconductor hosts with magnetic backgrounds (mostly AFM). However, in contrast to nonmagnetic hosts, whether magnetic coupling between TM impurities can be enhanced by an AFM lattice background has not been investigated systematically. If the magnetic exchange interaction between impurities can be enhanced by the AFM background, the impurity concentration required to achieve collective ferromagnetism/ferrimagnetism could be reduced. This could be helpful to avoid the clustering of dopants. Moreover, two nearest cations often share opposite spin orientations in AFM lattices,[42,43] favoring the uniform distribution of FM-coupled magnetic dopants. TM doping of AFM host semiconductors could,

a)Author to whom correspondence should be addressed. Electronic mail: zhaoyj@scut.edu.cn. Tel: +86-20-87110426; Fax: +86-20-87112837.

 © 2013 AIP Publishing LLC

Downloaded 04 Sep 2013 to 222.201.152.89. This article is copyrighted as indicated in the abstract. Reuse of AIP content is subject to the terms at: http://jap.aip.org/about/rights_and_permissions

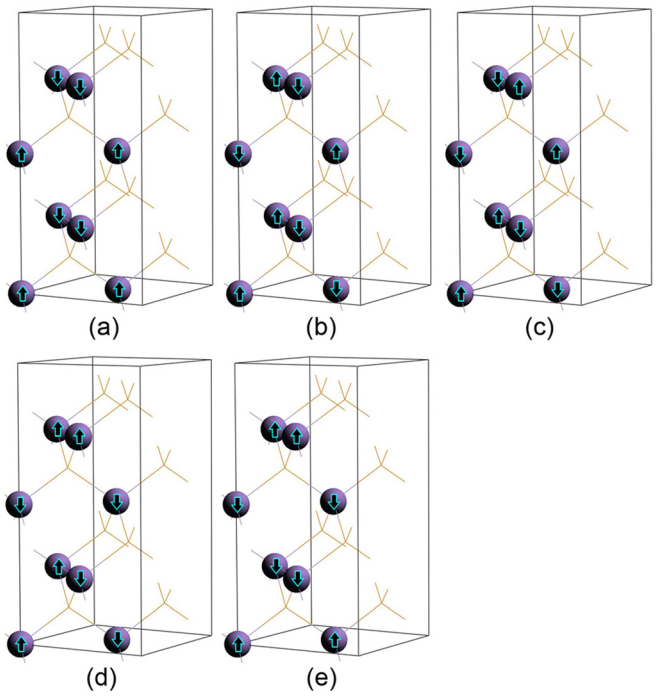

FIG. 1. Five AFM spin configurations (a)–(e) of a ZB Mn_8Te_8 system in a $1 \times 1 \times 2$ supercell. The purple balls represent Mn ions, with up and down arrows indicating spin orientation.

therefore, be a new approach to the realization of RT ferromagnetism/ferrimagnetism, although various physical issues need to be addressed.

In this paper, we theoretically investigated the structural stability and magnetic coupling of TMs (TM = V, Cr, Fe, Co, and Ni) in nonmagnetic hosts (ZnTe and CdTe) and in an AFM host (ZB MnTe). We found that the MnTe background degrades the clustering tendencies of V, Cr, Fe, and Co and remarkably enhances the magnetic coupling of Fe, Co, and Ni, in comparison with those in nonmagnetic hosts.

II. COMPUTATION METHODS

This work was performed using the Vienna *ab-initio* simulation package (VASP) based on density functional theory (DFT)[44,45] with a projector-augmented wave method.[46] The spin-polarized generalized gradient approximation of the Perdew–Wang 1991 formulas (GGA PW91)[47] was employed to describe the exchange correlations between the valence electrons. An energy cutoff for the plane wave basis was set to 320 eV for all studied systems. Integration in the reciprocal spaces was conducted in a k-mesh of $3 \times 3 \times 3$ for the 64-atom supercells because the total energy differences converged within 10 meV in a test calculation that used a $5 \times 5 \times 5$ k-mesh. It is well-known that the $3d$ levels of TM may not be well described by GGA in the strong-correlated systems, in particular, TM oxides. Nevertheless, the most interesting cases (Fe doping in ZnTe, CdTe, and MnTe) are also investigated by the GGA + U approach here, with U = 4 and 6 eV for Fe and Mn, following the earlier literatures [Refs. 48–50].

Both ZnTe and CdTe have a ground state in the ZB crystal lattice with optimized lattice parameters of 6.191 and 6.601 Å, respectively. For each nonmagnetic host, TM pairs of three structural configurations; the nearest neighbor (NN, $\sqrt{2}a/2$), the second NN (a), and the farthest separation ($\sqrt{3}a$) in a $2 \times 2 \times 2$ supercell, were considered. The configurations for the MnTe host are much more complicated because its magnetic background introduces nonequivalence for the TM pair configurations of the first and second neighbors in a 64-atom cell. This will be discussed later following the investigation of the ground magnetic state of MnTe.

III. RESULTS AND DISCUSSION

A. Stable TM pair configurations in ZB MnTe host

ZB MnTe, which was first prepared by molecular beam epitaxy (MBE) in 1989,[51] is a meta-stable phase with an observed lattice constant of 6.34 Å. Its reported energy gap is 3.19 eV,[52] much greater than that of NiAs-type MnTe (1.3 eV, c.f. Ref. 53). An earlier theoretical study[54] indicated that magnetic configurations with exactly half spin-up and half spin-down Mn ions in each tetrahedral unit are more energetically favored than other configurations in ZB MnTe. To confirm the most stable magnetic configuration in a pure ZB MnTe, we have studied five spin configurations in a 16-atom supercell. The first three spin configurations contain no net magnetic moment in any tetrahedra, while the fourth configuration contains two tetrahedra of (3↑,↓), (↑,3↓) Mn ions, and the fifth configuration contains two tetrahedra of 4↑ and 4↓ Mn ions (c.f. Fig. 1). These five configurations are hereafter denoted as AFM-I, AFM-II, AFM-III, AFM-IV, and AFM-V, as shown in $1 \times 1 \times 2$ (Mn_8Te_8) supercells in Figs. 1(a)–1(e). The calculated relative energies and structural parameters are listed in Table I. AFM-III, which can be described as a superlattice with Mn spin altering along $G = \langle 201 \rangle$ every two layers, is the most stable among the five configurations. The AFM-I and -II configurations have similar total energies (higher than that of AFM-III by 40 and

TABLE I. Comparison of five AFM spin configurations of Mn_8Te_8. E_0 is the total energy of each configuration with respect to that of AFM-III configuration. a_0 is the optimized crystal constant. d_{Mn-Te} is the distance between the TM impurity and its four nearest anions, Te. The energies in brackets are calculated with GGA + U method at fixed tetrahedral lattice of $a = 6.34$ Å, $c/a = 1$.

	AFM-I	AFM-II	AFM-III	AFM-IV	AFM-V
E_0/meV	40 (5)	16 (3)	***0 (0)***	201 (27)	772 (100)
a_0/Å	6.287	6.226	6.240	$a_0 = 8.851 \neq b_0$	$a_0 = 8.951 \neq b_0$
$2c_0/a_0$	1.96	2.02	2.00	1.58	1.40
d_{Mn-Te}/Å	2.70	2.70–2.71	2.70	2.68–2.73	2.72–2.74
Lattice	Tetrahedral	Tetrahedral	Tetrahedral	Orthorhombic	Orthorhombic

Downloaded 04 Sep 2013 to 222.201.152.89. This article is copyrighted as indicated in the abstract. Reuse of AIP content is subject to the terms at: http://jap.aip.org/about/rights_and_permissions

16 meV per cell, respectively), as well as similar lattice parameters and Mn-Te bond lengths. The AFM-IV and AFM-V configurations, which contain tetrahedral structures with net magnetic moments, are clearly energetically unfavorable by 201 and 772 meV per cell, respectively in comparison with that of AFM-III. In addition, a great structural distortion occurred in the latter two configurations. For instance, c_0/a_0 decreases from the 1.0 of a standard tetrahedral structure to around 0.7–0.8, with the symmetry changing to orthorhombic after full relaxation. The Mn-Te bond lengths also varied in a greater relative range of 2.68–2.74 Å, compared with 2.70 Å in configuration AFM-III. To confirm the stable magnetic configuration of MnTe, we also conducted GGA + U calculations. Here, we adopted a fixed tetrahedral lattice with experimental crystal parameters of $a = 6.34$ Å and $c/a = 1$for the GGA + U calculation since the lattice would experience an unreasonable deviation from the experimental lattice within GGA + U approach. The calculated energy differences between various configurations are also listed in Table I, it is clear that ZB MnTe still favors the AFM-III configuration, though the energy difference is much smaller that the corresponding GGA results. This is largely due to the different treatment of the lattice by GGA and GGA + U calculations. As a result, AFM-III MnTe with optimized a_0 (6.240 Å) and c_0/a_0 (1.00) is adopted for all following TM doping studies.

The 64-atom MnTe host supercell was constructed by doubling the $1 \times 1 \times 2$ (Mn_8Te_8) supercell (AFM-III) along the [100] and [010] directions. As shown in Fig. 2, there are three nonequivalent spin configurations for a TM (TM = V, Cr, Fe, Co, and Ni) pair in the first and second NN due to the magnetic background of the AFM-III configuration, which are noted with O-1, O-2, O-3, and O-A, O-B, O-C, respectively. For example (c.f. Fig. 2), the magnetic alignment of A-1-B is ↑-↓-↑, while B-2-C and A-3-C have different scenarios of ↑-↑-↓ and ↑-↓-↓, respectively, though these three configurations are structurally equivalent. The calculated energies of the various configurations are listed in Table II, with that of the most stable spin configuration set to zero for each type of TM impurity. The results indicate that different

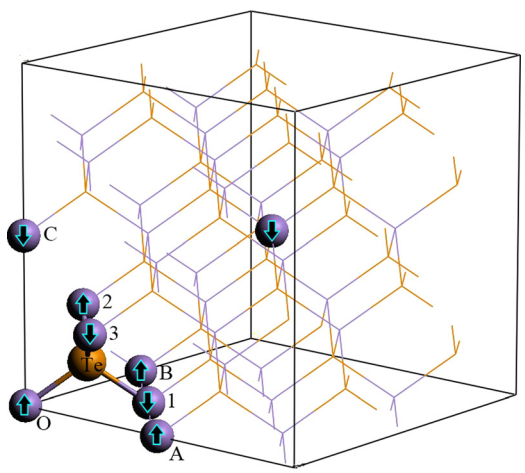

FIG. 2. Nonequivalent substitutional cation sites with TM pairs distributed in the nearest neighbors (configurations O-1, O-2, and O-3) and next nearest neighbors (configurations O-A, O-B, and O-C) in the ZB MnTe host.

TABLE II. Total energy differences of MnTe:TM systems with TM pair configurations at a separation of $d_{pair} = \sqrt{3}a$, and the nonequivalent configurations of $d_{pair} = \sqrt{2}a/2$ and $d_{pair} = a$. For each dopant pair, the total energy is relative to the most stable configuration, which is set to zero. The GGA + U calculation for O-A of case *a* for MnTe:Fe is hard to be converged, and thus denoted with a dash.

System energy/meV		V	Cr	Fe (GGA)	Fe (GGA + U)	Co	Ni
	O-1	27	***0***	29	6	42	262
	O-2	***0***	33	88	9	***0***	***0***
Case $\sqrt{2}a$ /2	O-3	9	18	21	32	42	246
	O-A	170	195	264	-	38	287
	O-B	168	195	***0***	4	39	311
Case *a*	O-C	269	208	23	***0***	36	330
Case $\sqrt{3}a$	/	260	169	25	1	43	343

TM pairs may have different stable spin configurations. For example, in the first *NN* configurations, V, Co, and Ni are stable at the O-2 configuration, while Cr pairs favor the O-1 and Fe pairs favor the O-3 configuration. The GGA + U results for MnTe:Fe are also listed in Table II. It indicates that the Fe pairs favor the next NN configuration according to both GGA and GGA + U calculations, though the detailed configurations are different, i.e., O-C for GGA + U and O-B for GGA, respectively. Meanwhile, the energies difference between configurations O-B and O-C is negligible in GGA + U calculation (~1 meV), while it is 23 meV in GGA calculation. Configuration O-A of MnTe:Fe is the most unstable configuration among the next NN Fe pairs in GGA, while it is even hard to be converged in GGA + U calculation. After determining the stable structural configuration of every TM pair, we will further discuss their clustering and magnetic coupling behaviors in an AFM-III MnTe host with respect to that in ZnTe and CdTe.

B. Electronic structure of TM in MnTe, ZnTe, and CdTe hosts

The electronic structure of TMs in non-magnetic ZB structures has been well studied.[8] Here, we found that the electronic configuration of a TM impurity in a MnTe host follows the same rule as in non-magnetic hosts, satisfying the high spin configurations we summarized in Ref. 8 (c.f. Fig. 3). In tetrahedral crystal field, the 3*d* levels of the TM impurity split into a triplet t_{2g} and a doublet e_{2g}. Subsequently, the t_{2g} levels will interact with the dangling *p* levels of neighboring anions, thereby forming bonding and anti-bonding levels, i.e., $t^{b}_{2g\pm}$ and $t^{anti}_{2g\pm}$ (where plus and minus indicate spin orientation). The arrangements of the coupled levels are similar to each other for all the considered TM impurities, as shown in Fig. 3(b). The $t^{b}_{2g\pm}$ and e_{2g+} levels are deep in energy and fully occupied, followed sequentially by t^{anti}_{2g+}, e_{2g-}, and t^{anti}_{2g-} as energy increases. These hybrid levels are gradually occupied as the number of valence electrons increase, leading to an open t^{anti}_{2g+} shell configuration for both substitutional V and Cr impurities, and open e_{2g-}, closed e_{2g-}, and open t^{anti}_{2g-} shells for Fe, Co, and Ni, respectively. For the NN pairs, V, Cr, and Ni are coupled ferromagnetically because they have an open t_{2g} shell, while Fe and Co

Downloaded 04 Sep 2013 to 222.201.152.89. This article is copyrighted as indicated in the abstract. Reuse of AIP content is subject to the terms at: http://jap.aip.org/about/rights_and_permissions

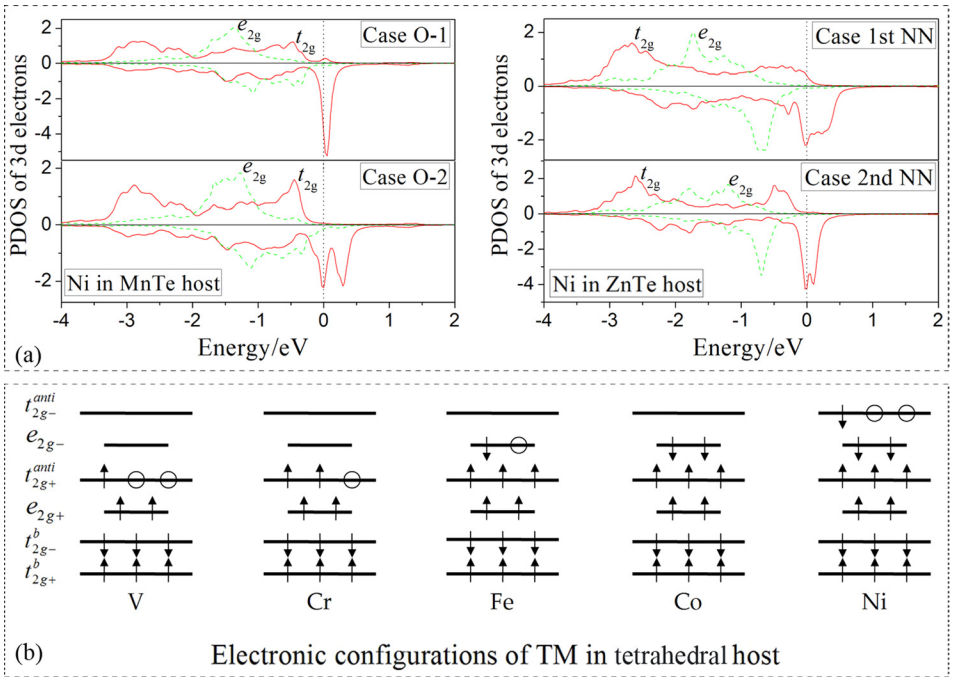

FIG. 3. (a) Partial density of states of Ni *3d* electrons in ZnTe and MnTe hosts, with t_{2g} and e_{2g} levels represented by red solid and green dashed lines, respectively. (b) Configurations of TM 3*d* electrons in tetrahedral hosts. The up and down arrows represent spin-polarized *d* electron occupations while the circles represent unoccupied TM *d* band levels.

are coupled antiferromagnetically with a closed t_{2g} shell configuration. Fig. 3(a) shows the partial density of states (PDOS) of Ni in ZnTe and MnTe hosts for the later discussion of clustering and magnetic coupling of Ni pairs, while the PDOS of other TMs in all three hosts are not shown here because their main features are illustrated in Fig. 3(b). As shown in Fig. 4(a), the total densities of states of MnTe:Fe in configuration *a* based on GGA + U calculations show definite energy band gaps (~2.69 eV) in both the spin channels. The GGA + U obtained electronic levels of MnTe:Fe and ZnTe:Fe also obey the rule well in general, though the occupied e_{2g+} (d_{Z^2}) is moving down and even below the t^b_{2g+} levels as shown in Figs. 4(b) and 4(c). Nevertheless, the GGA + U calculated e_{2g-} levels of Fe keep half occupied, in line with the GGA results.

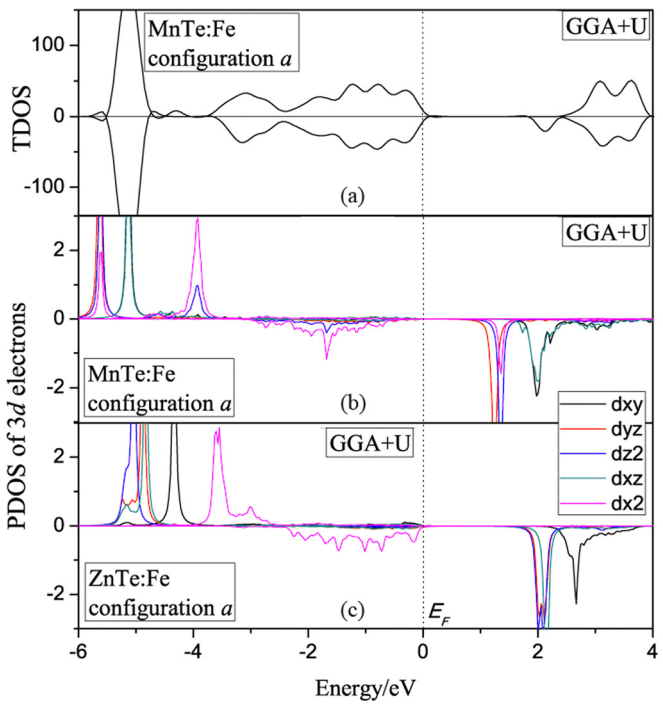

FIG. 4. GGA + U calculated (a) total densities of states of MnTe:Fe, (b) partial densities of states of MnTe:Fe, (c) partial densities of states of ZnTe:Fe for the next NN configuration.

C. Clustering trend

As mentioned above, TMs, especially Mn, often act as magnetic dopants in non-magnetic semiconductor systems. Clustering or secondary phases often accompany TM impurities in doped conventional semiconductors, leading to difficulties of intrinsic magnetism in tetrahedral systems. Here, we focus on exploring new possible approaches to reduce the clustering tendency of TM dopants in the AFM-III-type ZB MnTe host. Energetically, the clustering tendency of impurities in a given host can be described by an energy difference, such as clustering energy, between configurations with differently separated impurities. We took the system of the corresponding NN configuration, i.e., $d_{pair} = \sqrt{2}a/2$ as a reference, and set its energy to zero. Positive clustering energy implies a clustering tendency of the TM dopants, while negative values favor uniform configurations.

The calculated clustering energies of TMs in ZnTe and CdTe hosts are shown in Fig. 5(a) (highlighted in blue). It is clear that TM impurities doped in CdTe generally have a weaker clustering energy than that of those in ZnTe. This is expected to be related to the different TM pair distance, since CdTe and ZnTe are similar to each other both chemically and structurally. The greatest clustering energy difference (111 meV) appears at V pairs separated by $\sqrt{3}a$, while the least (14 meV) appears at Ni pairs separated by $\sqrt{3}a$. To further confirm the correlation between the host lattice constant and the clustering energies, we investigated the clustering energy of TMs in ZnTe and CdTe with lattice constants artificially varied by ±2%, i.e., 6.067 Å (−2%) and 6.315 Å (+2%) for ZnTe, as well as 6.469 Å (−2%) and 6.733 Å

Downloaded 04 Sep 2013 to 222.201.152.89. This article is copyrighted as indicated in the abstract. Reuse of AIP content is subject to the terms at: http://jap.aip.org/about/rights_and_permissions

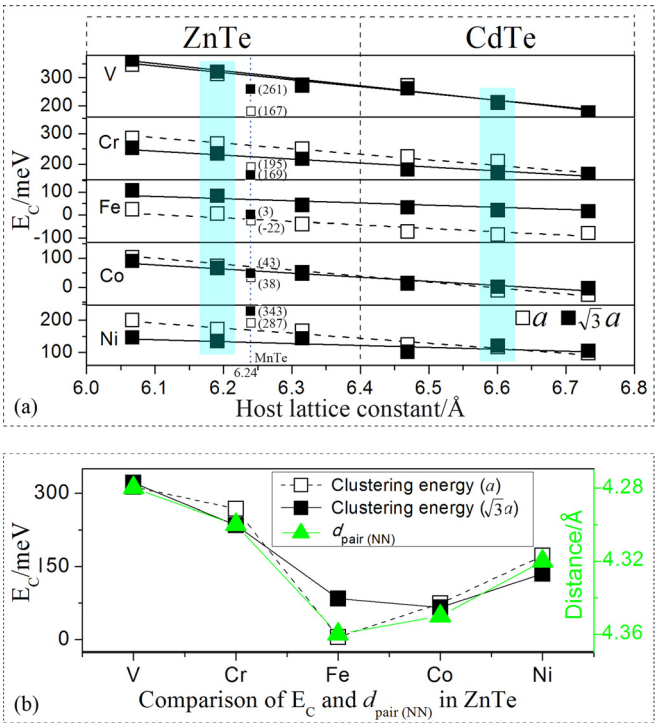

FIG. 5. (a) Clustering energies of TM impurities in nonmagnetic ZnTe and CdTe hosts (highlighted in blue), as well as for lattices artificially varied by ±2%. The open and solid squares represent the clustering energies of a and $\sqrt{3}a$ configurations, respectively, with respect to the NN configuration. Clustering energies of TM impurities in MnTe are also shown for comparison. (b) Comparison of clustering energies and TM distance for the NN configuration for various TMs in the ZnTe host (similar correlation is found for CdTe and MnTe hosts). Red triangles represent the distance of TM pairs in NN.

(+2%) for CdTe. A nearly linear decreasing trend was observed, within a tolerance of 20 meV, for the clustering energy of TM pairs as a function of the host lattice constant (c.f. Fig. 5). We concluded that the clustering tendency of TM impurities varies inversely with the host lattice constant. It could be understood that the decrease of TM-TM interaction is more significant in the first neighbor configuration than that in configurations with greater pair distance, reducing the clustering tendency of the TM impurities. Based on GGA + U calculation, the clustering energies of the next NN configurations of Fe pairs are in line with the GGA results well, varying inversely with the host lattice constant. Interestingly, the GGA + U calculated clustering energies of Fe in configuration $\sqrt{3}a$ are more than 1200 meV, much greater than that from GGA. It implies that the farthest configurations of Fe pairs are strongly unfavored in the nonmagnetic hosts with consideration of the Hubbard U correction. Meanwhile, the GGA + U calculated clustering energies of the farthest Fe pairs still changes linearly with the lattice constant within a deviation of 60 meV, implying a good size effect.

In the nonmagnetic hosts, the first neighbor distance of the TM ions is not necessarily the same for a given host because of structural relaxation. In fact, we found that the clustering energies are closely related to the distance of doped TMs of their NN configuration as the impurity varies from V to Ni. Exemplified with the ZnTe host, as shown in Fig. 5(b), the strongest clustering behavior appears for the V pair with a clustering energy of 313 and 321 meV for the a and $\sqrt{3}a$ configurations, respectively, corresponding to a NN pair distance of 4.28 Å. From V to Ni, the clustering energy reaches a minimum at Fe, at which the NN pair distance is the greatest at 4.36 Å, with a clustering energy of 5 and 84 meV for the a and $\sqrt{3}a$ configurations, respectively. From Fe to Ni, the pair distance decreases from 4.36 to 4.32 Å, while the clustering energy rises again to 172 and 135 meV for the a and $\sqrt{3}a$ configurations, respectively.

For V and Cr, their neighboring four Te ions are pushed outward by about 0.02 Å, because their 2+ ionic radius is greater than that of Zn. Meanwhile, the TM-Te-TM angle decreases from 109.5 to ~107°, therefore leading to a closer first NN TM pair distance. For Fe and Co, the neighboring four Te ions are contracted inward by about 0.04 Å, with the TM-Te-TM angle increasing from 109.5 to ~111°. This finally leads to a NN TM pair distance of 4.35–4.36 Å. The distance between Ni and Te is about 2.55 Å, with a TM-Te-TM angle of 114°, which corresponds to a NN TM pair distance of 4.32 Å. The variation of the TM-Te-TM angles is also expected to be related to the magnetic coupling enhancement of the TM pairs according to superexchange theory.[55]

MnTe and ZnTe have similar lattice constants of 6.240 and 6.191 Å, respectively. According to the size effect discussed above, the clustering energy difference in MnTe and ZnTe of each TM impurity is expected to be within 10 meV because their lattice constant difference is <1%. In fact, the total clustering energy of a TM (except Ni) in a MnTe host is generally much lower than that in a ZnTe host (roughly corresponding to the size effect in Fig. 5). The difference is up to 146 meV for V in the second NN, and is much greater than the lattice size effect (~10 meV) even for the least case, 23 meV for a Co pair of $\sqrt{3}a$. Following the GGA + U results, the size effects of clustering energies for Fe pairs in MnTe are 61 and 1268 meV for configurations a and $\sqrt{3}a$, respectively, strikingly higher than the corresponding total clustering effects (−28 and −31 meV, respectively). It clearly implies that the AFM background in MnTe plays a critical role in the reduction of clustering trend.

Here, we attempted to decompose the clustering tendency of TM pairs in MnTe into the contributions from the crystal lattice size and the AFM background. We defined the contribution from the crystal lattice size as E_S^C, which can be obtained from the nearly linear relation between the clustering energy and the lattice constant, as discussed earlier. The contribution of the Mn AFM background, E_M^C, can then be obtained as

$$E_M^C = E_C - E_S^C,$$

where E_C is the total clustering energy. Greater negative E_M^C indicates a stronger reduction in clustering degree, while a positive value indicates an enhancement by the Mn AFM background.

The calculated contributions of the size effects and the Mn AFM background to the clustering tendency of all studied impurity TMs in the MnTe host are shown in Fig. 6. The behavior of the size effect for the variation in TM impurities from V to Ni in MnTe is similar to that in the ZnTe host,

Downloaded 04 Sep 2013 to 222.201.152.89. This article is copyrighted as indicated in the abstract. Reuse of AIP content is subject to the terms at: http://jap.aip.org/about/rights_and_permissions

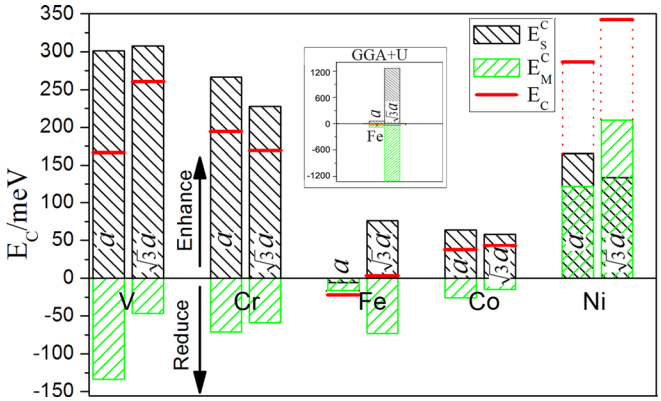

FIG. 6. Total and decomposed clustering energies (with respect to the NN configuration) of MnTe:TM systems, with configuration indicated by separation distance. Red line segments represent total clustering energies, while black and green shadow bars represent the size and Mn background effects, respectively. Positive values indicate clustering tendency, while negative values indicate a trend towards relatively uniform distribution. The corresponding GGA + U results for MnTe:Fe are shown in the inserted plot.

with its strength descending to a minimum around Fe and Co, and rising again for Ni. Regarding the total effect of clustering in MnTe, Fe and Co, especially Fe, have a relatively weak clustering tendency (disappeared for Fe of next NN configuration), as well as relatively weak size effects (from −5.82 to 76.3 meV) and weak Mn AFM background effects (from −73.3 to −14.8 meV). The effect of the Mn AFM background on the clustering energy degrades from V to Co but has an abrupt enhancement for Ni, in which E_M reaches about 122 meV (configuration of a) and 210 meV (configuration $\sqrt{3}a$). The reduction in the effects of Mn for V to Co is also related to the variation of TM pair distance of their first NN configuration, similar to the size effect in ZnTe illustrated in Fig. 5(b). Ni has a rather unusual behavior on the Mn effect with a greater clustering energy. Further analysis will be given in the latter part of section 3.3 for a better understanding of this irregular behavior. According to the GGA + U results, the contributions of the AFM background effect to the clustering tendency of Fe in MnTe reaches −89 and −1299 meV for configurations a and $\sqrt{3}a$, respectively. The clustering trend for MnTe:Fe disappears as the clustering energies turn to be negative, −28 and −31 meV for the configurations of a and $\sqrt{3}a$, respectively, well in line with GGA results.

D. Magnetic coupling of the TM pairs

When magnetic impurities effectively interact with each other to form FM or Ferri coupling, systems will have a collective magnetic moment, which is critical to spin-polarized electron transport in DMS materials. A high doping concentration is often required to maintain effective magnetic coupling between TM impurities. However, high-concentration impurity doping often leads to clustering or secondary-phase behaviors, and fails to give intrinsic magnetism. Therefore, enhancement of the effective interaction distance and the coupling intensity between magnetic impurities has become a critical issue for high-quality DMS materials.

We defined the exchange energy as the difference between AFM coupling and FM coupling of TM pairs for given configurations as

$$E_{EX} = E_{AFM} - E_{FM},$$

where E_{AFM} represents the system energy with two antiferromagnetically coupled TM impurities, while E_{FM} represents the system energy of the FM case.

The mechanism of magnetic coupling between two TM dopants becomes more complicated with the introduction of the Mn AFM background of the MnTe host. We decomposed the total exchange energy into two contributing parts, the crystal lattice (size effect) and the Mn background effects, similar to the decomposition of the clustering energy in Sec. III B. We define the Mn background effect as

$$E_M^{EX} = E_{EX} - E_S^{EX},$$

where E_S^{EX} represents the size effect on the exchange energy of the TM impurity. Of note, similar to the nonmagnetic hosts, only the FM coupling of TM impurities in MnTe contributes to the collective magnetic moments because the magnetic moments are canceled out in the case of AFM-coupled TM impurities.

As shown in Fig. 7 (highlighted in blue), we have found that the differences of exchange energies between ZnTe and CdTe hosts are within 80 meV for all considered TM impurity configurations, with the greatest appearing at the $\sqrt{3}a$ Fe pair of (77 meV). In fact, the difference falls in the 50-meV range except for the $\sqrt{3}a$ Fe pair and the NN Cr pair. To further investigate the size effect of the host crystals, we have compared the exchange energy of TM pairs in the series of nonmagnetic hosts with various artificial lattice constants as done in Sec. III B. The differences in E_{EX} still fall in the range of 80 meV as the lattice constant increases from 6.067 to 6.733 Å, as shown in Fig. 6, except for the $\sqrt{3}a$ Fe pair, in which the deviation reaches up to 297 meV with exchange energies of −91 and 206 meV in the case of 6.315 and 6.469 Å, respectively. Nevertheless, the host lattice size has no remarkable effect on the exchange energies of TM impurities in general. It is also the case for Fe from GGA + U calculations, where the exchange energies change linearly in general when the host lattice crystal constants varied from

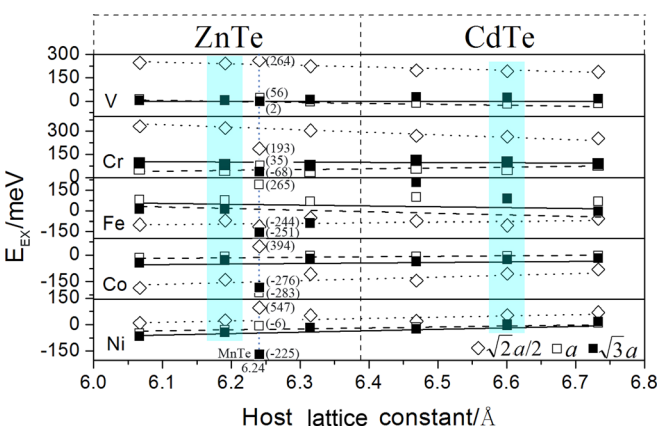

FIG. 7. Magnetic exchange energies, $E_{EX} = E_{AFM} - E_{FM}$, of TM pairs in ZnTe and CdTe hosts (highlighted in blue), as well for lattices artificially varied by ±2%. Open diamonds represent the $\sqrt{2}a$ /2 configuration, while the open and solid squares represent the a and $\sqrt{3}a$ configurations, respectively. E_{EX} of TM pairs in MnTe are also illustrated for comparison.

Downloaded 04 Sep 2013 to 222.201.152.89. This article is copyrighted as indicated in the abstract. Reuse of AIP content is subject to the terms at: http://jap.aip.org/about/rights_and_permissions

6.067 Å to 6.733 Å, with the largest deviation of 40 meV for configuration $\sqrt{3}a$ at lattice of 6.191 Å.

The total exchange energies, as well as the decomposed size and Mn background effects are illustrated in Fig. 8. The differences in exchange energies between MnTe and ZnTe hosts are expected to be within 10 meV when only the size effect is considered because their crystal constant differs by no more than 1%. In fact, the calculated magnitude of the TM exchange energy in MnTe is remarkably greater than that in ZnTe for most TM impurities (roughly corresponding to the size effect in Fig. 8). In the case of Fe, for example, the magnitude of its exchange energy is enhanced by 173 meV (AFM enhancement), 190 meV (FM enhancement), and 241 meV (AFM enhancement) with respect to that in the ZnTe host for the first NN, the second NN, and the farthest configurations of Fe pairs, respectively. According to the GGA + U calculations, the size effects for Fe pairs are −29, −15, and −15 meV for configurations $\sqrt{2}a/2$, a, and $\sqrt{3}a$, respectively. The corresponding Mn AFM background effects are −21, 89, and −259 meV, respectively, showing remarkable AFM enhancements for configurations $\sqrt{2}a/2$ and $\sqrt{3}a$, and an FM enhancement for configuration of a, in line with GGA results.

Although the effect of the Mn background on the exchange coupling is complicated, we have found that it generally enhances, either ferromagnetically or antiferromagnetically, the coupling strength of TM pairs, except for Cr, as well as V $\sqrt{3}a$ and Ni a configurations (c.f. Fig. 8). In the following, we will pay more attention to the cases of V ($\sqrt{2}a/2$, and a), Fe (a), Co ($\sqrt{2}a/2$), and Ni ($\sqrt{2}a/2$, and a) because the Mn background provides an obvious FM coupling enhancement for them. In contrast to the size effect, the Mn AFM background has a relatively small effect on V and Cr, but much stronger effects for Fe, Co, and Ni (except configuration a), with remarkable enhancements in Co (538 meV) and Ni (515 meV) pairs in the $\sqrt{2}a/2$ configuration. The most interesting case, however, is the Fe pair in the second NN configuration, in which the Mn background not only stabilizes its relative uniform distribution, but also enhances its FM coupling.

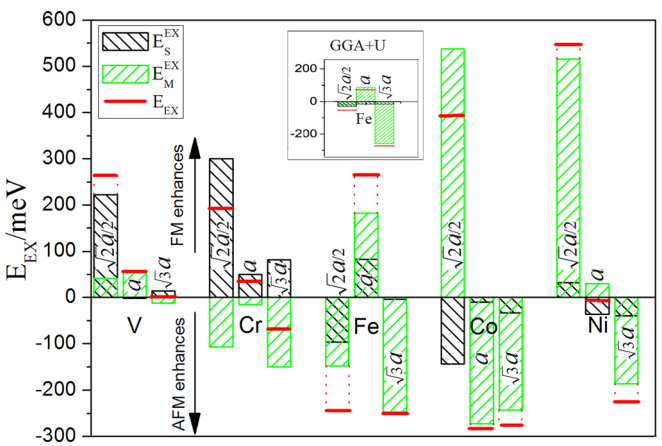

FIG. 8. Total and decomposed exchange energies of MnTe:TM systems, with pair configurations indicated by separation distance. Red line segments represent total exchange energies, while black and green shadow bars represent the size and Mn background effects, respectively. Positive and negative exchange energies correspond to favoring of FM and AFM coupling, respectively. The corresponding GGA + U results for MnTe:Fe are shown in the inserted plot.

Meanwhile, the Mn background introduces a remarkable FM coupling enhancement for Co and Ni of the first NN configuration (c.f. Fig. 8). Because a closed shell e_{2g-} (c. f. Fig. 3) is expected for Co in II–VI hosts, the Co pair is expected to favor AFM coupling. Interestingly, it turns out to strongly favor FM in MnTe in the presence of the Mn AFM background (c.f. Fig. 7). A delocalization of t_{2g-}^{anti} levels was found for Co of the NN configuration in MnTe when its PDOS is compared with that in the ZnTe host. An overlap of e_{2g-} and t_{2g-}^{anti} due to the Mn background makes electron transition from e_{2g-} to t_{2g-}^{anti} possible in Co, and thus leads to a stable FM coupling phase for the Co pair because the t_{2g-}^{anti} shell is no longer fully closed.[8]

Ni has an open t_{2g-}^{anti} shell, which corresponds to a favorable weak FM coupling in ZnTe, because its anti-bonding levels are mostly occupied. It is unusual that both its clustering energy and exchange energy are remarkably enhanced when the Mn AFM background is introduced. By comparing the system energies of various Ni pair configurations, we found that the energy of O-2 in FM coupling is lower than that of other configurations by 250–350 meV (c.f. Table II). This directly leads to the high clustering energy and highly enhanced FM coupling behaviors. For further discussion, we have illustrated the PDOS of Ni *3d* levels in MnTe and ZnTe in Fig. 3(a). For the MnTe host, a delocalization of t_{2g-}^{anti} near the Fermi level was found for the most stable Ni pair configurations (O-2 of FM coupling), but is not available for other configurations. Because Ni has an open t_{2g-}^{anti} shell, the delocalization lowers system energy by pushing t_{2g+}^{anti} into a deeper level. As a result, the FM coupled O-2 configuration is much lower in energy than other Ni configurations in MnTe. For the ZnTe host, however, the delocalization of t_{2g-}^{anti} appears in all the configurations, though it is more remarkable in the FM-coupled NN pair configuration, leading to relatively comparable energies for the Ni configurations.

IV. CONCLUSION

First-principles calculations were conducted for the clustering and magnetic coupling of TM (V, Cr, Fe, Co, and Ni) pairs in ZB MnTe and compared with those of non-magnetic ZnTe and CdTe hosts. We found that the clustering of doped TMs is slightly enhanced as the lattice constant decreases in non-magnetic hosts, while it is clearly degraded by the AFM background of MnTe, except TM = Ni. The AFM background of MnTe also remarkably enhances the magnetic coupling of doped Fe, Co, and Ni (except for a configuration of a) pairs, either ferromagnetically or antiferromagnetically. The strong impact of the AFM background on the clustering and magnetic coupling of doped impurities may provide a new approach to develop high T_C magnetic semiconductors with intrinsic magnetism.

ACKNOWLEDGMENTS

This work was supported by the NSFC (Grant No. 11174082). Computer time at the National Supercomputing

Downloaded 04 Sep 2013 to 222.201.152.89. This article is copyrighted as indicated in the abstract. Reuse of AIP content is subject to the terms at: http://jap.aip.org/about/rights_and_permissions

Center in Shenzhen (NSCCSZ) and the ScGrid of the Supercomputing Center, Computer Network Information Center of CAS is gratefully acknowledged.

[1]H. Ohno, Science **281**, 951 (1998).
[2]H. Ohno, D. Chiba, F. Matsukura, T. Omiya, E. Abe, T. Dietl, Y. Ohno, and K. Ohtani, Nature (London) **408**, 944 (2000).
[3]A. Continenza, G. Profeta, and S. Picozzi, Phys. Rev. B **73**, 035212 (2006).
[4]S. Shen, X. Liu, Y. J. Cho, J. K. Furdyna, M. Dobrowolska, Y. H. Hwang, and Y. H. Um, Appl. Phys. Lett. **94**, 142507 (2009).
[5]K. Sato, L. Bergqvist, J. Kudrnovský, P. H. Dederichs, O. Eriksson, I. Turek, B. Sanyal, G. Bouzerar, H. Katayama-Yoshida, V. A. Dinh, T. Fukushima, H. Kizaki, and R. Zeller, Rev. Mod. Phys. **82**, 1633 (2010).
[6]M. Kobayashi, Y. Ishida, J. I. Hwang, G. S. Song, A. Fujimori, C. S. Yang, L. Lee, H. J. Lin, D. J. Huang, C. T. Chen, Y. Takeda, K. Terai, S. I. Fujimori, T. Okane, Y. Saitoh, H. Yamagami, K. Kobayashi, A. Tanaka, H. saito, and K. Ando, New J. Phys. **10**, 055011 (2008).
[7]R. A. de Groot, F. M. Mueller, P. G. van Engen and K. H. J. Buschow, Phys. Rev. Lett. **50**, 2024 (1983).
[8]Y.-J. Zhao, P. Mahadevan, and A. Zunger, J. Appl. Phys. **98**, 113901 (2005).
[9]T. Dietl, H. Ohno, F. Matsukura, J. Cibert, and D. Ferrand, Science **287**, 1019 (2000).
[10]T. Dietl, H. Ohno, and F. Matsukura, Phys. Rev. B **63**, 195205 (2001).
[11]L. Bergqvist, K. Sato, H. K. Yoshida, and P. H. Dederichs, Phys. Rev. B **83**, 165201 (2011).
[12]K. Y. Ko, IEEE Tran. Magn. **45**, 2428 (2009).
[13]I. Stefaniuk, M. Bester, and M. Kuzma, J. Phys.: Conf. Ser. **104**, 012010 (2008).
[14]Y. B. Li, Y. Q. Zhang, N. K. Sun, Q. Zhang, D. Li, J. Li, and Z. D. Zhang, Phys. Rev. B **72**, 193308 (2005).
[15]K. Nakamura, T. Ito, and A. J. Freeman, Phys. Rev. B **72**, 064449 (2005).
[16]J. N. Goncalves, V. S. Amaral, and J. G. Correia, Phys. Rev. B **83**, 104421 (2011).
[17]W. Kim, I. J. Park, H. J. Kim, W. Y. Lee, S. J. Kim, and C. S. Kim, IEEE Tran. Magn. **45**, 2424 (2009).
[18]L. Ottaviano, A. Continenza, G. Profeta, G. Impellizzeri, A. Irrera, R. Gunnella, and O. Kazakova, Phys. Rev. B **83**, 134426 (2011).
[19]D. W. Rench, P. Schiffer, and N. Samarth, Phys. Rev. B **84**, 094434 (2011).
[20]B. Hennion, W. Szuszkiewicz, E. Dynowska, E. Janik, and T. Wojtowicz, Phys. Rev. B **66**, 224426 (2002).
[21]K. J. Kim, J. H. Lee, H. J. Lee, J. B. Yoon, M. H. Jung, W. Kim, S. J. Kim, and C. S. Kim, J. Korean Phys. Soc. **53**, 742 (2008).
[22]L. F. Zhu and B. G. Liu, Phys. Status Solidi B **246**, 1094 (2009).
[23]S. F. Qi, F. X. Jiang, J. P. Fan, H. Wu, S. B. Zhang, G. A. Gehring, Z. Y. Zhang, and X. H. Xu, Phys. Rev. B **84**, 205204 (2011).
[24]X. L. Lin, S. S. Yan, M. W. Zhao, S. J. Hu, X. X. Yao, C. Han, Y. X. Chen, G. L. Liu, Y. Y. Dai, and L. M. Mei, J. Appl. Phys. **107**, 033903 (2010).
[25]D. Huang, Y.-J. Zhao, D. H. Chen, and Y. Z. Shao, Appl. Phys. Lett. **92**, 182509 (2008).
[26]K. R. Kittilstved, D. A. Schwartz, A. C. Tuan, S. M. Heald, S. A. Chambers, and D. R. Gamelin, Phys. Rev. Lett. **97**, 037203 (2006).
[27]K. Ueda, H. Tabata, and T. Kawai, Appl. Phys. Lett. **79**, 988 (2001).
[28]H. Alawadhi, I. Miotkowski, V. Souw, M. McElfresh, A. K. Ramdas, and S. Miotkowska, Phys. Rev. B **63**, 155201 (2001).
[29]C. E. Arrondo, J. P. Conde, and A. Ayuela, Phys. Rev. B **79**, 155319 (2009).
[30]K. Sato, W. Schweika, P. H. Dederichs, and H. K. Yoshida, Phys. Rev. B **70**, 201202(R) (2004).
[31]K. G. Roberts, M. Varela, S. Rashkeev, S. T. Pantelides, S. J. Pennycook, and K. M. Krishnan, Phys. Rev. B **78**, 014409 (2008).
[32]Editorial, Nature Mater. **9**, 951 (2010).
[33]Interview with N. Samarth, Nature Mater. **9**, 955–956 (2010).
[34]Interview with S. Chambers, Nature Mater. **9**, 956–957 (2010).
[35]A. Zunger and S. Lany, Physics **3**, 53 (2010).
[36]T. Dietl, Nature Mater. **9**, 965–974 (2010).
[37]J. J. Zhang, W. Q. Jie, L. J. Luan, T. Wang, and D. M. Zeng, J. Electron. Mater. **37**, 1158 (2008).
[38]S. A. Touat, F. Litimein, A. Tadjer, and B. Bouhafs, Physica B **405**, 625 (2010).
[39]P. Banerjee and B. Ghosh, Appl. Surf. Sci. **255**, 4689 (2009).
[40]N. H. Long, J. Supercond. Nov. Magn. **20**, 473 (2007).
[41]N. H. Long, M. Ogura, and H. Akai, J. Appl. Phys. **106**, 123905 (2009).
[42]J. M. Hastings, N. Elliott, and L. M. Corliss, Phys. Rev. **115**, 13 (1959).
[43]H. Sato, T. Mihara, A. Furuta, M. Tamura, K. Mimura, N. Happo, M. Taniguchi, and Y. Ueda, Phys. Rev. B **56**, 7222 (1997).
[44]G. Kresse and J. Hafner, Phys. Rev. B **47**, 558 (1993).
[45]G. Kresse and J. Furthmüller, Phys. Rev. B **54**, 11169 (1996).
[46]G. Kresse, Phys. Rev. B **59**, 1758 (1999).
[47]J. P. Perdew and Y. Wang, Phys. Rev. B. **45**, 13244 (1992).
[48]L. Wang, T. Maxisch, and G. Ceder, Phys. Rev. B. **73**, 195107 (2006).
[49]A. Schrön, C. Rödl, and F. Bechstedt, Phys. Rev. B. **82**, 165109 (2010).
[50]A. Schrön, C. Rödl, and F. Bechstedt, Phys. Rev. B. **86**, 115134 (2012).
[51]S. M. Durbin, J. Han, O. Sungki, M. Kobayashi, D. R. Menke, R. L. Gunshor, Q. Fu, N. Pelekanos, A. V. Nurmikko, D. Li, J. Gonsalves, and N. Otsuka, Appl. Phys. Lett. **55**, 2087 (1989).
[52]Y. R. Lee, A. K. Ramdas, and R. L. Aggarwal, Phys. Rev. B **38**, 10600 (1988).
[53]J. W. Allen, G. Lucovsky, and J. C. Mikkelsen, Jr., Solid State Commun. **24**, 367 (1977).
[54]S. H. Wei and A. Zunger, Phys. Rev. B. **48**, 6111 (1993).
[55]H. A. Kramers, Physica **1**, 182 (1934).

Downloaded 04 Sep 2013 to 222.201.152.89. This article is copyrighted as indicated in the abstract. Reuse of AIP content is subject to the terms at: http://jap.aip.org/about/rights_and_permissions